Aerodynamic Parameter Estimation Using Reconstructed Turbulence Measurements

Jared A. Grauer*
NASA Langley Research Center, Hampton, Virginia, 23681

A classical method for reconstructing atmospheric turbulence from onboard measurements of airdata and inertial sensors was improved and implemented for real-time computation. The reconstructed turbulence measurements were then included in a system identification analysis to estimate nondimensional stability and control derivatives in a longitudinal short period model using the maximum likelihood equation-error method in the frequency domain with Fourier-transform data. Flight test results using a subscale transport-type airplane showed that the power spectra for the reconstructed vertical gusts resembled the von Kármán turbulence model. Flight data in moderate and severe turbulence exhibited a decorrelation of the modeling data that increased the accuracy of parameter estimation results using the reconstructed turbulence. In particular, pitch rate and angle-of-attack rate derivatives could both be identified from flight data about straight and level flight without special maneuvers or prior information.

Nomenclature

a_x, a_y, a_z	=	accelerometer measurements, g
b	=	wingspan, ft
C_a	=	nondimensional aerodynamic coefficient for $a = Z$ or m
cov	=	covariance operator
$\bar{c}$	=	mean aerodynamic chord, ft
f	=	frequency, Hz
g	=	gravitational acceleration, ft/s^2
$I_{xx}, I_{yy}, I_{zz}, I_{xz}$	=	moments and product of inertia, slug-ft^2
j	=	imaginary number, $= \sqrt{-1}$
M_T	=	pitching moment from propulsion, ft-lbf
m	=	aircraft mass, slug
p, q, r	=	angular rates, rad/s

*Research Engineer, Dynamic Systems and Control Branch, MS 308, Associate Fellow AIAA.

$\bar{q}$ = dynamic pressure, lbf/ft^2

$\Re$ = real part

S = wing reference area, ft^2

$s(.)$ = standard error

t = time, s

u, v, w = translational velocities, ft/s

V = true airspeed, ft/s

x, y, z = body-axis coordinates, ft

α = angle of attack, rad

β = sideslip angle, rad

Δ = perturbation

δ_e = elevator deflection, rad

σ = standard deviation

ϕ, θ, ψ = Euler angles, rad

ω = frequency, rad/s

$|.|$ = magnitude

$\angle$ = phase angle, deg

Subscripts

0 = reference value

Superscripts

† = complex conjugate transpose

$\hat{}$ = estimated value

$^{-1}$ = matrix inverse

^{T} = matrix transpose

$\dot{}$ = time derivative

$\tilde{}$ = Fourier transform

$\bar{}$ = average value

I. Introduction

Atmospheric turbulence is often present during flight tests. Because turbulence affects the motion of the aircraft but is not directly measured, the accuracy of most system identification analyses degrades when turbulence levels are significant. For example, the maximum likelihood output-error method using time-domain data [1], assumes all inputs are accurately measured. When significant turbulence is present, matches to measured output data become poor and parameter estimates incur biases and large uncertainties.

The most common and simple approach to mitigate the adverse effects of turbulence on system identification is to only conduct flight tests in calm air when the effects of turbulence are negligible. However, this practice can result in schedule delays in testing and additional costs. In cases where the flight data cannot be repeated, such as during accident investigations or expensive flight test experiments, the effects of turbulence can lead to inaccurate estimation results. If testing in turbulence cannot be avoided, an effective technique is to increase amplitudes of excitation inputs to reduce the relative effects of turbulence [2], although care must be taken to keep the aircraft responses small enough to maintain modeling assumptions and to stay within maneuver load limits.

Another approach is to alter the identification method to account for the turbulence. In the maximum likelihood filter-error method [1] and nonlinear state estimation [3], turbulence can be considered process noise or an additional state driven by white noise. These methods can be difficult to use because of increased complexity, convergence problems, and unrealistic assumptions about turbulence. In contrast, the maximum likelihood equation-error method [2, 4] is a simpler approach that allows for process noise on the aircraft model and is routinely used for aircraft system identification. Equation error was used in Ref. [2] to obtain satisfactory estimates of stability and control derivatives for flight in turbulence. References [5, 6] further investigated sources of error and colored noise using this method.

This paper presents a different approach in which turbulence was reconstructed from other measurements and included as a known input in the identification. The reconstruction was based on a classical technique that combines measured airdata and inertial information, but was improved in this work for the purpose of system identification by using more accurate equations and a frequency-domain transform. The approach was demonstrated using flight test data for a subscale airplane to estimate stability and control derivatives in the short-period model using the equation-error method with Fourier-transform data. The main contributions of this paper are the improved turbulence reconstruction during maneuvering flight and the discussion about its application to aerodynamic parameter estimation.

The organization of this paper is as follows. Section II describes the mathematical representation of the turbulence. Section III discusses the aerodynamic model for the short period mode approximation considering vertical gusts. Section IV presents the classical and enhanced methods for turbulence reconstruction. Section V briefly summarizes parameter estimation in the frequency domain using equation error. Section VI describes the T-2 subscale airplane. Section VII presents analysis results using flight test data. Lastly, Section VIII provides further discussion and conclusions.

All of the software used in this work was written in MATLAB®. Some of the software used for the data analysis, collinearity assessment, Fourier transforms, and parameter estimation tasks came from the software toolbox called System IDentification Programs for AirCraft, or SIDPAC [7], which is associated with Ref. [4].

II. Turbulence Definition

The terms turbulence and gusts are used in this paper to refer to any motion of the atmosphere relative to an inertial reference frame. The development is focused on the vertical and apparent pitching components of turbulence, but the approach is similar for other components.

The convention for turbulence used in Refs. [8–10] is followed in this paper, in which the vertical gust component w_g is positive when the wind moves downward around the aircraft, in the direction of the positive body z-axis. With regard to the modeled aerodynamics, this motion is equivalent to the airplane moving upwards with an equal velocity through a still atmosphere. Small $w_g > 0$ therefore create the approximate angle of attack increment

$$\alpha_g \simeq -\frac{w_g}{u} \tag{1}$$

As the aircraft traverses a turbulence field, an apparent rotational motion of the atmosphere relative to the aircraft manifests from the gust gradient. Assuming the turbulence field is frozen in time, the resulting pitch rate gust is approximated as

$$q_g = -\frac{\partial w_g}{\partial x} = -\frac{\partial w_g/\partial t}{\partial x/\partial t} \simeq -\frac{\dot{w}_g}{u} \simeq \dot{\alpha}_g \tag{2}$$

for large spatial wavelengths of turbulence relative to the aircraft size, and for small changes in forward speed. This definition of q_g uses a sign convention consistent with α_g.

III. Aerodynamic Model

The aerodynamic forces and moments are represented as first-order Taylor series expansions about a reference flight condition using stability and control derivatives. Perturbations to the nondimensional aerodynamic coefficients involving short-period motions for a rigid-body airplane are postulated in the body axes [8] as

$$\Delta C_a = C_{a_w}\left(\Delta w - \Delta w_g\right) + C_{a_{\dot{w}}}\left(\dot{w} - \dot{w}_g\right)\frac{\bar{c}}{2u_0} + C_{a_q}\left(q - q_g\right)\frac{\bar{c}}{2u_0} + C_{a_{\delta_e}}\Delta\delta_e \tag{3}$$

Equation (3) applies to both the vertical force coefficient ($a = Z$) and to the pitching moment coefficient ($a = m$). The aircraft mass, geometry, airspeed, and dynamic pressure are assumed to be constant. By substituting Eqs. (1) and (2) into (3), the aerodynamic coefficients can alternatively be expressed for low angles of attack in the stability axes [11] as

$$\Delta C_a = C_{a_\alpha}\left(\Delta\alpha + \Delta\alpha_g\right) + C_{a_{\dot\alpha}}\left(\dot\alpha + \dot\alpha_g\right)\frac{\bar c}{2V_0} + C_{a_q}\left(q - \dot\alpha_g\right)\frac{\bar c}{2V_0} + C_{a_{\delta_e}}\Delta\delta_e \tag{4}$$

In Section VII, the unknown stability and control derivatives in Eq. (4) are estimated using flight test data and the equation-error method described in Section V.

IV. Turbulence Reconstruction

A classical method for reconstructing turbulence, sometimes called the "flow vane technique," was explored in Ref. [12], formalized in Refs. [13, 14], and revisited in other works. The fundamental concept is to remove the motion of the airplane from measured air flow data to recover the motion of the atmosphere, or turbulence.

The linearized output equation for the angle of attack measurement using an air flow vane is

$$\alpha_v = \alpha - \frac{x_\alpha}{V}q + \alpha_g \tag{5}$$

The first term, α, is the angle of attack at the center of mass. Reference [13] suggested integrating vertical accelerometer measurements a_z to obtain α. The second term in Eq. (5) is due to an offset x_α of the vane from the center of mass along the body x-axis, and can be computed from measurements of V and q. The last term, α_g, can then be reconstructed because the other terms are known. In contrast to other model-based estimation approaches, no assumptions on the stochastic character of the turbulence or dynamics of the aircraft are imposed.

The flow vane technique is simple and has been used successfully to characterize the spectral content of turbulence components from flight data. However, the technique applies simplifications in the vane measurement equation and in the computation of α which reduces its accuracy. Consequently, flight tests were typically conducted in straight and level flight with control effectors mechanically fixed to minimize the command response of the airplane [12]. This approach is helpful for reconstructing turbulence but is detrimental for a system identification analysis, which usually requires movement of the control effectors.

The classical technique was improved for system identification analysis from maneuvering flight in three ways. First, the nonlinear vane output equation was used, instead of the linearized version in Eq. (5), to improve modeling fidelity. Assuming rigid-body dynamics and negligible forward gusts compared to the airspeed, the angle of attack vane output is

$$\alpha_v = \arctan\left(\frac{w - x_\alpha q + y_\alpha p - w_g}{u - y_\alpha r + z_\alpha q}\right) \tag{6}$$

where y_α and z_α are the locations of the vane along the body y- and z-axes relative to the center of mass. By rearranging

Eq. (6) for w_g and substituting it into Eq. (1), the angle of attack gust is

$$\alpha_g = -\frac{1}{u}\left[w - x_\alpha q + y_\alpha p - \tan\alpha_v \left(u - y_\alpha r + z_\alpha q\right)\right] \tag{7}$$

This reconstruction is similar to Eq. (5) but retains the trigonometric nonlinearity in the vane measurement, as well as contributions from all angular rates. Turbulence can excite all axes of the aircraft motion, making the angular rate contributions significant, particularly for smaller aircraft with lower mass and inertia [15]. For the flight data discussed later in Section VII, about 30% of the variation in the reconstructed turbulence from the wing-tip vane data was attributed to the angular rate terms.

Second, the classical technique was improved by solving the nonlinear aircraft kinematic equations [4, 16]

$$\dot{u} = rv - qw + ga_x - g\sin\theta \tag{8a}$$

$$\dot{v} = pw - ru + ga_y + g\sin\phi\cos\theta \tag{8b}$$

$$\dot{w} = qu - pv + ga_z + g\cos\phi\cos\theta \tag{8c}$$

for u, v, and w using numerical integration and measured data, and then substituting the results into Eq. (7). The initial conditions can be taken as

$$u(t_0) = V(t_0)\cos\alpha(t_0)\cos\beta(t_0) \tag{9a}$$

$$v(t_0) = V(t_0)\sin\beta(t_0) \tag{9b}$$

$$w(t_0) = V(t_0)\sin\alpha(t_0)\cos\beta(t_0) \tag{9c}$$

This step was more accurate than the classical practice of integrating a_z measurements and allows for arbitrary motion of the airplane and movement of the control effectors.

Third, the reconstructed turbulence was transformed into the frequency domain using a Fourier transform, as discussed in Section V. The transformation removes the low-frequency drift in the solution to Eq. (8), and consequently in Eq. (7), which is due to measurement noise and bias errors in the sensor data. The transformation also removes the high-frequency content which contains unmodeled dynamics and noise. The transformation is only performed over the modeling bandwidth of interest, which produces a relatively small number of data points for an efficient analysis in the frequency domain.

These enhancements improved the accuracy of the reconstructed turbulence and facilitated its inclusion as a measured input for system identification in the frequency domain. These improvements can also be applied to reconstructions of forward and lateral gust components. Rotational gusts cannot be directly reconstructed in this way and have to be derived from the translational gusts as in Eq. (2) because gyroscopes measure inertial information rather than air-relative information. The primary cost for reconstructing turbulence using this approach is high-quality and low-noise instrumentation.

V. Parameter Estimation

The aerodynamic models in Eq. (4) are linear functions of the stability and control derivatives to be estimated, and can be cast in the standard form

$$\mathbf{z} = \mathbf{y} + \mathbf{v} \tag{10a}$$

$$= \mathbf{X}\boldsymbol{\theta} + \mathbf{v} \tag{10b}$$

where $\mathbf{z}$ is the dependent variable, $\mathbf{y}$ is the model output, $\mathbf{v}$ is the error, $\mathbf{X}$ is the matrix of explanatory variables, and $\boldsymbol{\theta}$ is the vector of model parameters.

The dependent variables considered here are computed from measured data [4] as

$$C_Z = \frac{mg}{\bar{q}S} a_z \tag{11a}$$

$$C_m = \frac{I_{yy}}{\bar{q}S\bar{c}} \left[\dot{q} + \left(\frac{I_{xx} - I_{zz}}{I_{yy}} \right) pr + \frac{I_{xz}}{I_{yy}} \left(p^2 - r^2 \right) - M_T \right] \tag{11b}$$

Equation (11) represents the nonlinear, rigid-body, longitudinal motion of the aircraft and accounts for time variations in quantities such as mass and airspeed. The explanatory variables are computed from measured data, and the model parameters are the stability and control derivatives. For example using C_Z,

$$\mathbf{z} = \begin{bmatrix} C_Z(t_1) & C_Z(t_2) & \dots & C_Z(t_N) \end{bmatrix}^T \tag{12a}$$

$$\mathbf{X} = \begin{bmatrix} \Delta\alpha(t_1) + \Delta\alpha_g(t_1) & \left[\dot{\alpha}(t_1) + \dot{\alpha}_g(t_1)\right] \frac{\bar{c}}{2V_0} & \left[q(t_1) - \dot{\alpha}_g(t_1)\right] \frac{\bar{c}}{2V_0} & \Delta\delta_e(t_1) \\ \Delta\alpha(t_2) + \Delta\alpha_g(t_2) & \left[\dot{\alpha}(t_2) + \dot{\alpha}_g(t_2)\right] \frac{\bar{c}}{2V_0} & \left[q(t_2) - \dot{\alpha}_g(t_2)\right] \frac{\bar{c}}{2V_0} & \Delta\delta_e(t_2) \\ \vdots & \vdots & \vdots & \vdots \\ \Delta\alpha(t_N) + \Delta\alpha_g(t_N) & \left[\dot{\alpha}(t_N) + \dot{\alpha}_g(t_N)\right] \frac{\bar{c}}{2V_0} & \left[q(t_N) - \dot{\alpha}_g(t_N)\right] \frac{\bar{c}}{2V_0} & \Delta\delta_e(t_N) \end{bmatrix} \tag{12b}$$

$$\boldsymbol{\theta} = \begin{bmatrix} C_{Z_\alpha} & C_{Z_{\dot{\alpha}}} & C_{Z_q} & C_{Z_{\delta_e}} \end{bmatrix}^T \tag{12c}$$

$$\mathbf{v} = \begin{bmatrix} v_Z(t_1) & v_Z(t_2) & \dots & v_Z(t_N) \end{bmatrix}^T \tag{12d}$$

over N time samples. A similar representation is used for C_m.

After terms in Eq. (10) are computed and assembled, modeling data are converted into the frequency domain. The next step is to remove a linear trend from the data that equates the endpoints of the time series to zero to improve the convergence of the Fourier transform [4, 17]. Then the Fourier integral

$$\tilde{z}(j\omega_k) = \int_0^T z(t)\, e^{-j\omega_k t}\, dt \tag{13}$$

is computed using the chirp z-transform over the time duration T and for frequency indices $k = 1, 2, \ldots, M$. The transform is applied with arbitrary frequency resolution and over the frequency bandwidth of interest. This yields a relatively low number of frequency-domain data samples to process during the estimation, but that have good signal-to-noise ratios, resulting in an efficient estimation. Because the data are detrended, biases and low-frequency drifts are removed from the data. Similarly, because frequencies above the modeling bandwidth are not used, high-frequency noise and unmodeled dynamics are automatically removed from the data.

The maximum likelihood equation-error solution to Eq. (10) using Fourier transform data minimizes the cost function

$$J(\boldsymbol{\theta}) = \frac{1}{2}\,(\tilde{\mathbf{z}} - \tilde{\mathbf{y}})^{\dagger}\,(\tilde{\mathbf{z}} - \tilde{\mathbf{y}}) \tag{14}$$

Because the estimation problem is decoupled, the estimation is performed twice: once for C_Z and once for C_m. The optimal solution to Eq. (14) for the model parameters is

$$\hat{\boldsymbol{\theta}} = \left[\Re\left(\tilde{\mathbf{X}}^{\dagger}\tilde{\mathbf{X}}\right)\right]^{-1}\Re\left(\tilde{\mathbf{X}}^{\dagger}\tilde{\mathbf{z}}\right) \tag{15}$$

The estimated parameter covariance matrix is

$$\mathrm{cov}(\hat{\boldsymbol{\theta}}) = \sigma^2\left[\Re\left(\tilde{\mathbf{X}}^{\dagger}\tilde{\mathbf{X}}\right)\right]^{-1} \tag{16}$$

where the equation-error variance can be estimated from the residuals [18] as

$$\hat{\sigma}^2 = \frac{(\tilde{\mathbf{z}} - \tilde{\mathbf{y}})^{\dagger}\,(\tilde{\mathbf{z}} - \tilde{\mathbf{y}})}{2T\,(f_M - f_1)} \tag{17}$$

The parameter standard errors are the square-roots of the diagonal elements in Eq. (16).

Equations (13) to (17) are formulated for batch estimation, after all the modeling data have been collected. Alternatively, the estimation can be performed in real time, during a flight test and as data are being collected. This is mechanized by reconstructing the turbulence at each time step and applying a recursive Fourier transform. The equation-error solution requires only small amounts of computational resources when performed in the frequency domain, and can be repeatedly applied at a feasible update rate. For more information on the equation-error approach and on real-time implementation, see Ref. [4].

Although the equation-error method using Fourier-transform data was described in this section, other methods could also be used for parameter estimation. However, time-domain methods must contend with drift in the reconstructed data, for example by including trend models or by high-pass filtering the data, and higher-frequency dynamics and measurement noise. The output-error method could also be applied, but can not generally run in real time. Using Fourier-transform data, output error is restricted to linear time-invariant state models, which is an assumption often violated for flight data in turbulence. Frequency response techniques could also be applied, but must contend with multiple correlated inputs and transient responses in the data.

VI. Test Aircraft

The T-2 Generic Transport Model (GTM) airplane, which is shown in Fig. 1, was used to demonstrate the approach. The T-2 is a 5.5% dynamically-scaled version of a transport-type aircraft, with twin jet engines mounted under the wings and retractable tricycle landing gear. Aircraft geometry and nominal mass properties are listed in Table 1. The nominal flight condition investigated was straight and level flight at about 5 deg angle of attack, 135 ft/s airspeed, and 1500 ft altitude.

Fig. 1 T-2 airplane (credit: NASA Langley Research Center).

The aircraft is instrumented with research-quality hardware, and was flown remotely from the Airborne Subscale Transport Aircraft Research (AirSTAR) flight-test facility. The instrumentation includes a micro inertial navigation system, an additional inertial measurement unit, and air data probes attached to booms mounted on each wingtip. Flight data were measured at 200 Hz, downsampled to 50 Hz, and digitally low-pass filtered to 16 Hz for analysis.

Flight test data for 23 maneuvers in various levels of turbulence from flights 15, 30, and 33 were analyzed. An example of one maneuver in severe turbulence is shown in Fig. 2. The elevator input was an orthogonal phase-optimized multisine [4], which contained power between 0.3 and 2.1 Hz. The flight data also included multisine inputs on the aileron and rudder, but only the longitudinal motion was examined in this paper. In comparison to the elevator multisine,

Table 1 T-2 aircraft geometry and nominal mass properties.

Symbol	Value	Unit
$\bar{c}$	0.915	ft
b	6.849	ft
S	5.902	ft^2
m	1.585	slug
I_{xx}	1.179	slug-ft^2
I_{yy}	4.520	slug-ft^2
I_{zz}	5.527	slug-ft^2
I_{xz}	0.211	slug-ft^2

pilot inputs were low in amplitude and frequency.

The turbulence level was quantified using the empirical metric $\sigma_{w\,[2\text{–}7\text{ Hz}]}$, which was introduced in Ref. [2] to measure the power in w between 2 and 7 Hz. The vertical component of velocity was used because the turbulence was most apparent in the vertical axis and was speculated to be the result of convection from diurnal heating. The range 2 to 7 Hz was selected because it was higher in frequency than the rigid-body dynamics but still contained appreciable content due to the turbulence. The metric correlated well with turbulence ratings from the pilot, who was flying the airplane from the ground using a heads-up display drawn from telemetered data and a map of the local terrain. Light, moderate, and severe turbulence were judged have $\sigma_{w\,[2\text{–}7\text{ Hz}]}$ values of approximately 0.2, 0.4, and 0.6 ft/s, respectively. Reference [2] discusses real-time computation of this metric from airspeed and angle of attack measurements using spectral density estimation and frequency binning. A different approach was employed here, where the detrended data were projected on a Fourier sine series [4, 17] and coefficients outside the 2–7 Hz bandwidth were discarded. The turbulence metric was computed as the standard deviation of the reconstructed signal. Applied to a Monte Carlo simulation, this technique produced turbulence metrics with less scatter than using the spectral density approach.

VII. Results

A. Turbulence Reconstruction

An example of turbulence reconstruction is shown in Fig. 3 for flight test data in severe turbulence. Figure 3(a) is the reconstruction in the time domain, whereas Fig. 3(b) is the reconstruction in the frequency domain, which is represented by Fourier transform magnitude and phase data. The modeling bandwidth was between 0.1 and 3.0 Hz, which included the short period mode (1 Hz), the elevator excitation, and the range for which the reconstructed turbulence had appreciable power. The reconstructed turbulence appeared similar to what would be used for simulation data [19], and had an exponential decrease in magnitude with increasing frequency.

The power spectra of reconstructed vertical gusts are shown for two levels of turbulence in Fig. 4. The spectra were

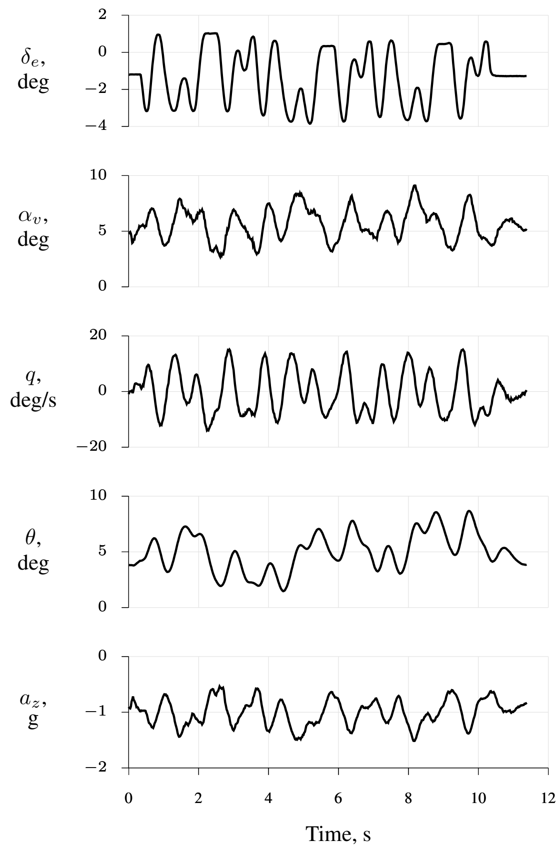

Fig. 2 Flight test data in severe turbulence.

computed using the one-sided periodogram [20]

$$G_{ww}(j\omega) = \frac{2}{T}|\tilde{w}_g(j\omega)|^2 \tag{18}$$

for each maneuver, and then averaged at each frequency over the ensemble. This computation was possible because the chirp z-transform allows for arbitrary specification of the analysis frequencies, regardless of the maneuver time duration. Unlike in Fig. 3, these results are shown up to the 25 Hz Nyquist frequency. The red and blue lines in Fig. 4 correspond to flight data in light and severe turbulence, and each consist of six averaged maneuvers having roughly the same turbulence level. The black trend lines fitted to estimated spectra over 1 to 16 Hz had an average slope -1.86 ± 0.26, which was in statistical agreement with the theoretical value of $-5/3$ or about -1.67 used in the von Kármán turbulence model [19].

B. Collinearity Analysis

When regressor data are nearly collinear or linearly dependent, an estimator cannot decipher between the effects, and resulting parameter estimates are biased with large uncertainties [4]. Pairwise correlation between two explanatory

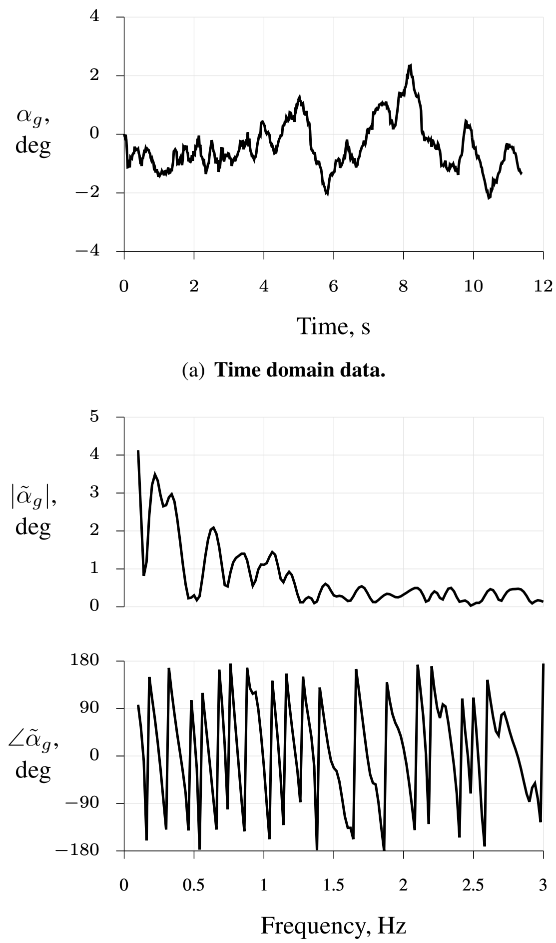

(a) **Time domain data.**

(b) **Fourier transform data.**

Fig. 3 Reconstructed angle-of-attack gust in severe turbulence.

variables, $\mathbf{x}_j$ and $\mathbf{x}_k$, is measured by the correlation coefficient

$$r_{jk} = \frac{\sum_{i=1}^{N} \left[x_j(t_i) - \bar{x}_j\right] \left[x_k(t_i) - \bar{x}_k\right]}{\sqrt{\sum_{i=1}^{N} \left[x_j(t_i) - \bar{x}_j(t_i)\right]^2 \sum_{i=1}^{N} \left[x_k(t_i) - \bar{x}_k(t_i)\right]^2}} \tag{19}$$

which ranges between ± 1. For flight dynamics analysis, correlations larger than 0.9 in absolute value are considered highly correlated and poor estimation results can be expected. Visually, data with high correlation values appear as nearly straight lines when the time series are plotted against each other.

Example plot matrices are shown in Fig. 5 for flight data in light and severe turbulence. The data used to generate these plots only contained power over the modeling bandwidth. The matrix diagonal labels the associated model parameters from Eq. (4), the lower triangle shows the pairwise correlation coefficients computed using Eq. (19), and the upper triangle shows cross plots of the time series.

For light turbulence, shown in Fig. 5(a), most pairs of explanatory variables had low correlations. Data for $C_{a_{\delta_e}}$ and

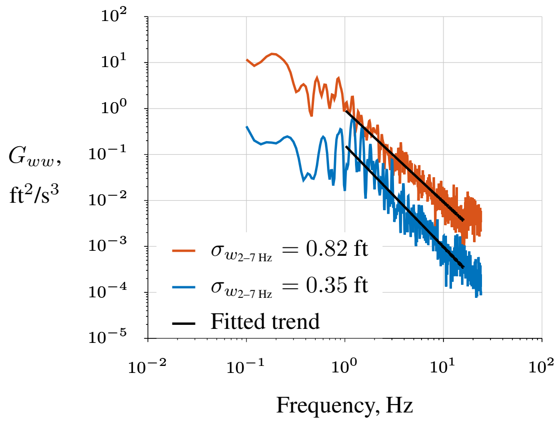

Fig. 4 Power spectra of reconstructed vertical gusts in light and severe turbulence.

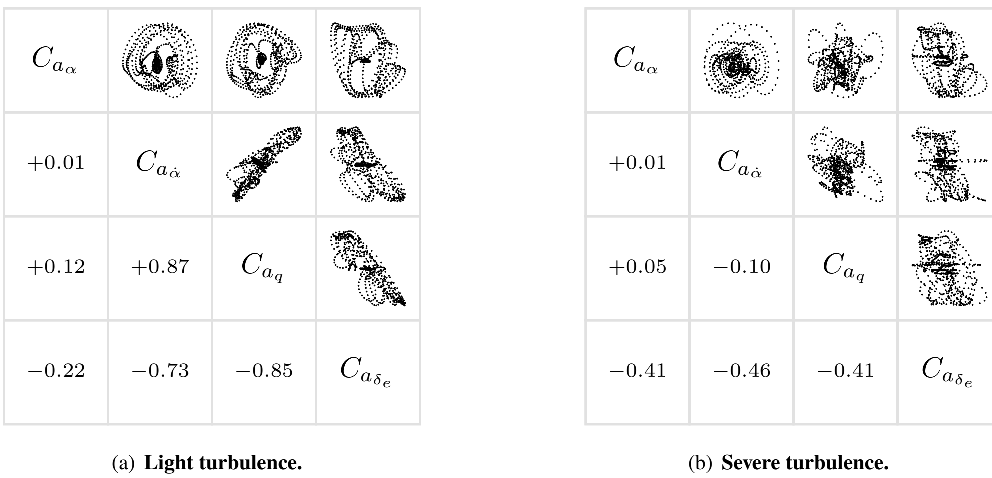

Fig. 5 Plot matrices of explanatory variables.

C_{a_q}, and also for $C_{a_{\delta_e}}$ and $C_{a_{\dot\alpha}}$, were moderately correlated. As expected, data for $C_{a_{\dot\alpha}}$ and C_{a_q} were highly correlated, which is why for maneuvers in straight and level flight these terms are typically lumped together as a single parameter $\bar{C}_{a_q}$ for estimation, or rather why special maneuvers or prior information are used [4, 21–23].

For severe turbulence, shown in Fig. 5(b), most of the parameter correlations decreased in absolute value. The only exception was data for C_{a_α} and $C_{a_{\delta_e}}$, but this correlation did not increase to a significant level. The reduction for $C_{a_{\dot\alpha}}$ and C_{a_q} was most significant, switching sign and becoming almost completely uncorrelated. Pairwise correlations for the 23 flight test maneuvers, which are shown as a function of turbulence level in Fig. 6, confirmed these trends. Larger changes in correlation were exhibited when the data were not restricted to the modeling bandwidth, but were attributed to higher-frequency noise and unmodeled dynamics.

Figures 5 and 6 indicate that some level of turbulence is useful for decorrelating the explanatory variables, which can lead to more accurate parameter estimates. This result is counter-intuitive because it is standard practice to conduct

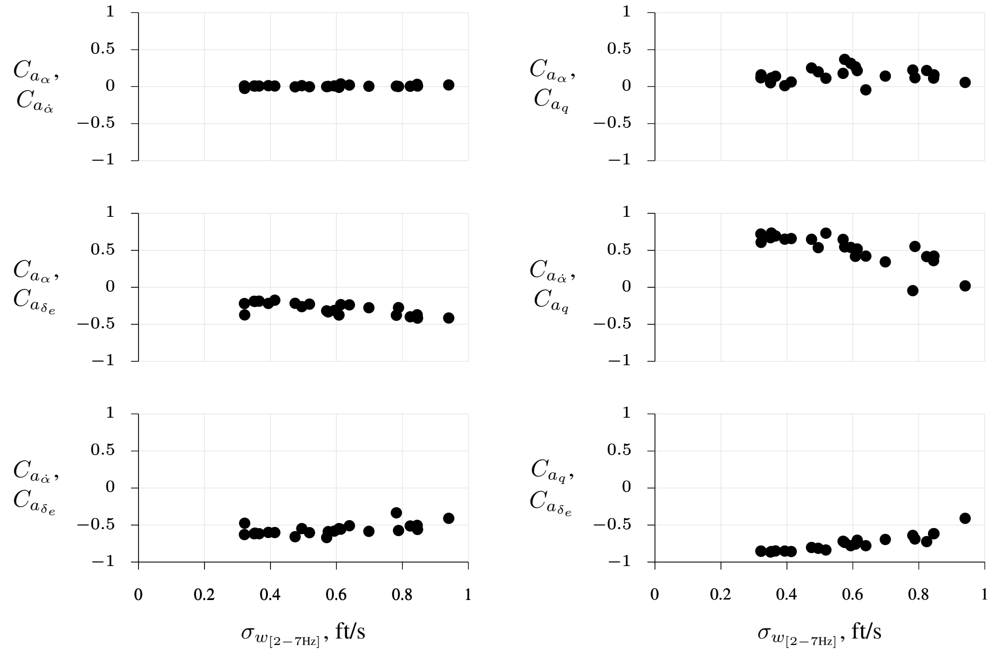

Fig. 6 Pairwise correlations for various turbulence levels.

flight tests in calm air, without turbulence. However, with accurate reconstructions of turbulence included in the system identification analysis, more accurate results can be obtained.

In addition to pairwise collinearity, multicollinearity was also examined, which is when one regressor resembles a linear combination of other regressors. Multicollinearity problems cannot always be detected using pairwise correlations and require other tests. Typical multicollinearity detection techniques [4] were applied and no multicollinearity was found.

C. Parameter Estimation

Equation-error parameter estimation was applied to the 23 flight test maneuvers, and results are given in Fig. 7 as a function of the turbulence level. Uncertainties on the model parameters are shown as $\pm 2\sigma$ error bounds.

Parameter estimates using the full model in Eq. (4) with reconstructed turbulence are shown as blue circles. All stability and control derivatives were estimated, and the estimates were generally consistent over the turbulence range. In particular, estimates of $C_{Z_{\dot\alpha}}$ and $C_{m_{\dot\alpha}}$, which are difficult to identify accurately, were generally consistent and were similar to the estimates -2.3 and -11.5, respectively, which were obtained using first-principles theory [24].

For comparison, the reduced aerodynamic model

$$\Delta C_a = C_{a_\alpha}\left(\Delta\alpha + \Delta\alpha_g\right) + \bar{C}_{a_q}\frac{q\bar{c}}{2V_0} + C_{a_{\delta_e}}\Delta\delta_e \tag{20}$$

was also used for estimation. This model corresponds to the normal case where turbulence is not reconstructed (but is

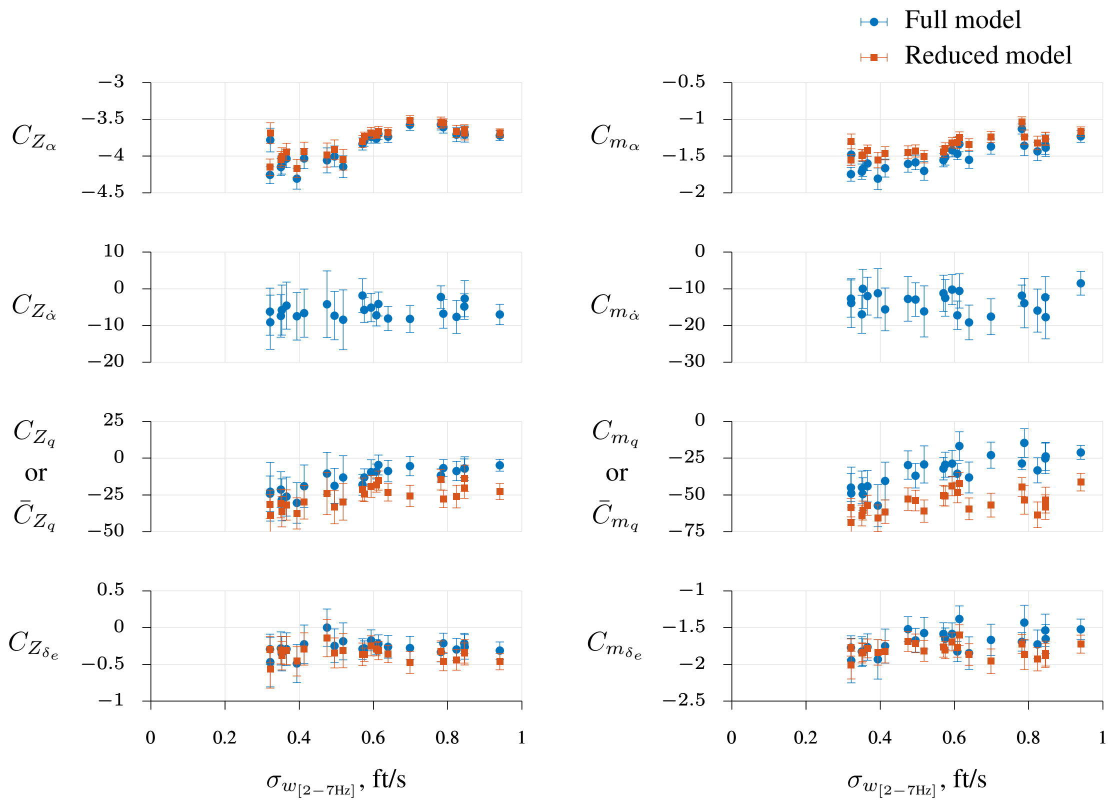

Fig. 7 Parameter estimates and 2σ uncertainties.

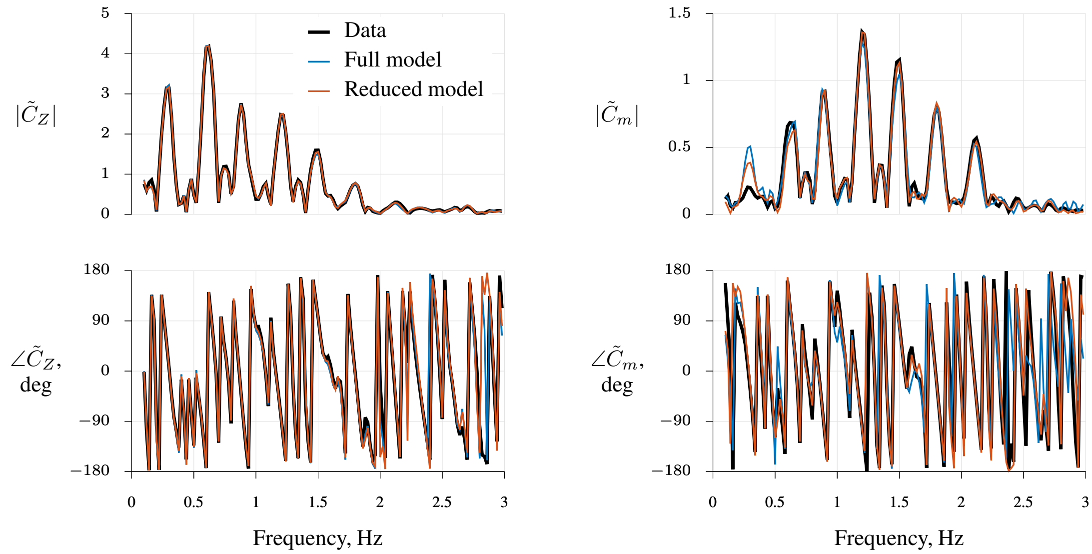

(a) Vertical force coefficient.

(b) Pitching moment coefficient.

Fig. 8 Equation-error fits to data from 14 maneuvers with $\sigma_{\mathrm{w}\,[2\text{–}7\ \mathrm{Hz}]} > 0.5$ ft/s.

still indirectly measured using the vane) and the stability derivative $\bar{C}_{a_q}$ is used to subsume the correlated angle of attack rate and pitch rate effects.

Parameter estimates using the reduced model are shown as red squares in Fig. 7. Most of the variation from $C_{a_{\dot{\alpha}}}$ was attributed to $\bar{C}_{a_q}$, although some was also absorbed into C_{a_α} and $C_{a_{\delta_e}}$, which changed those values relative to estimates using the full model.

For some parameters in the full model, particularly C_{Z_α}, small bias shifts, decreases in uncertainty, and less scatter in the estimates were exhibited for turbulence metrics above 0.5 ft/s. This is because the turbulence had become large enough to decorrelate the data and enable more accurate identification of the stability and control derivatives, as discussed in Section VII.B. This was also true for the reduced model because the primary effect of turbulence manifests in the α_g term, which is still measured with the flow vane and applied in the estimation, even without turbulence reconstruction.

Model fits to data from 14 maneuvers having $\sigma_{w\,[2\text{–}7\ \mathrm{Hz}]}$ above 0.5 ft/s are shown in Fig. 8 and the resulting parameter estimates and standard errors are given in Table 2. The two fits to C_Z are practically identical, each having $R^2 = 0.99$. The C_m data was fit slightly better by the reduced model than the full model, with coefficients of determination R^2 values of 0.98 and 0.94, respectively. The estimates of C_{a_α} and $C_{a_{\delta_e}}$ were similar between the two sets of models, and were in rough agreement with previous analyses [2, 23], but had statistical differences due to the different model structures and modeling data used.

A prediction maneuver using these two identified models is shown in Fig. 9. The flight condition was 4.5 deg angle of attack, 140 ft/s airspeed, and 1250 ft altitude, which was similar to the maneuvers used for identification. The

Table 2 Model parameters and standard errors identified from 14 maneuvers with $\sigma_{\mathrm{w}\,[2\text{–}7\ \mathrm{Hz}]} > 0.5$ ft/s.

Parameter θ	Full model $\hat{\theta} \pm s(\hat{\theta})$	Reduced model $\hat{\theta} \pm s(\hat{\theta})$
C_{Z_α}	-3.71 ± 0.01	-3.67 ± 0.01
$C_{Z_{\dot{\alpha}}}$	-5.74 ± 0.48	—
C_{Z_q}	-8.66 ± 0.82	-21.5 ± 0.88
$C_{Z_{\delta_e}}$	-0.26 ± 0.02	-0.36 ± 0.02
C_{m_α}	-1.39 ± 0.01	-1.28 ± 0.01
$C_{m_{\dot{\alpha}}}$	-13.1 ± 0.60	—
C_{m_q}	-27.0 ± 1.00	-50.7 ± 0.99
$C_{m_{\delta_e}}$	-1.63 ± 0.02	-1.79 ± 0.02

turbulence for this maneuver was light, with a turbulence metric of 0.28 ft/s. The maneuver included a small elevator doublet exciting the short period response. The identified model parameters in Table 2 were substituted into a state-space model of the short period dynamics and simulated using the measured elevator time history. Matches to the measured data were excellent and had R^2 values above 0.95 for all time histories. The modal characteristics of the two models at this condition were similar: the full model had short period damping 0.43 and natural frequency 6.4 rad/s (1.0 Hz), whereas the reduced model had damping ratio 0.50 and natural frequency 6.4 rad/s (1.0 Hz).

This prediction case demonstrates that the short period models, identified from data with turbulence metrics larger than 0.5 ft, both predict the aircraft motion well in lower amounts of turbulence. Other maneuvers involving rapid motions, takeoff, or landing could reveal differences between the two identified models.

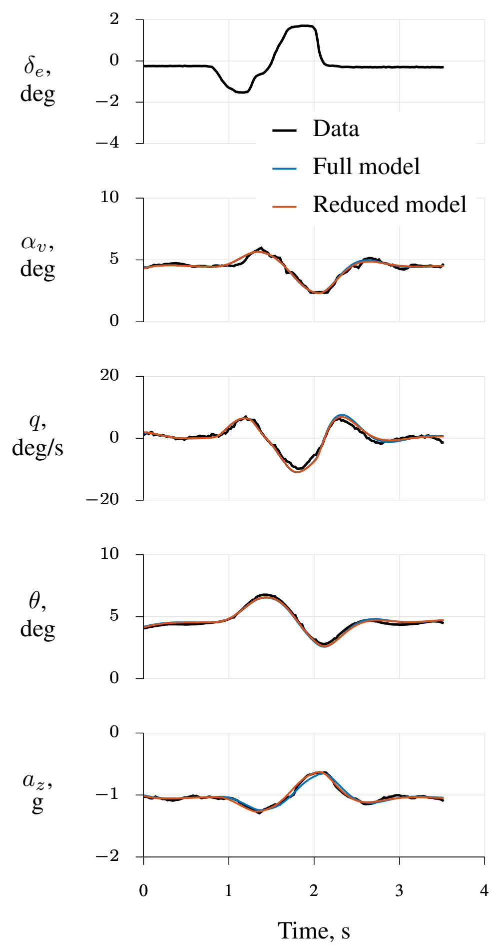

Fig. 9 Prediction case in light turbulence.

VIII. Conclusions

System identification of aircraft aerodynamic models using reconstructed turbulence measurements was investigated and discussed. A classical technique for turbulence reconstruction, based on airdata and inertial sensor measurements, was enhanced and applied to maneuvering flight. Nondimensional stability and control derivatives were estimated using the reconstructed measurements of turbulence and the maximum likelihood equation-error method in the frequency domain. Results were demonstrated using flight test data for the T-2 GTM subscale airplane. The main findings of this research can be summarized as:

1) The angle of attack increment from the gust was accurately reconstructed over 0 to 3 Hz from data in maneuvering flight.
2) For moderate and severe turbulence, explanatory variables became decorrelated which led to more accurate parameter estimates, including for $C_{m_{\dot{\alpha}}}$ and C_{m_q}.
3) Identification using turbulence reconstruction and the full model gave additional physical insight into the flight dynamics over the reduced model, but both models predicted the motion about straight and level flight in calm air equally well.

The primary advantage of the proposed approach is the simplicity in the analyses, both in the reconstruction of the turbulence and the parameter estimation. These methods are computationally simple but incorporate the coupled, nonlinear dynamics of the aircraft, and can be run in real time as data are collected during flight. Furthermore, these techniques alleviate the need to apply more complex algorithms for parameter estimation, such as nonlinear state estimators or the maximum likelihood filter-error method. The cost of this approach is high-quality instrumentation so that the turbulence can be accurately reconstructed and distinguished from other responses and measurement noise.

The proposed methods can be used for several applications. Turbulence can be computed in real time to expand flight testing opportunities with relaxed restrictions on turbulence levels. Although only vertical gusts and short-period dynamics were investigated in this paper, the approach could be extended to the other gust components and dynamics of the aircraft. The reconstructed turbulence measurements could also be used as inputs for a turbulence-suppression flight control system, or to develop custom models of turbulence for simulation purposes such as handling qualities analysis or training for flight in hazardous conditions associated with turbulence. Real-time turbulence measurements could be used to quantify the level of turbulence during a flight test, independent of the aircraft dynamics or a turbulence model, which would be useful in cooperative flights with multiple aircraft.

Acknowledgments

This research was supported by the NASA Advanced Air Transport Technology (AATT) Project. The T-2 flight data used was generated by the NASA Langley (LaRC) AirSTAR team under the NASA Aviation Safety Program, Vehicle Systems Safety Technologies (VSST) project.

References

[1] Maine, R., and Iliff, K., "Formulation and Implementation of a Practical Algorithm for Parameter Estimation with Process and Measurement Noise," *SIAM Journal on Applied Mathematics*, Vol. 41, No. 3, 1981, pp. 558–579. doi:10.1137/0141045.

[2] Morelli, E., and Cunningham, K., "Aircraft Dynamic Modeling in Turbulence," *Atmospheric Flight Mechanics Conference*, AIAA Paper 2012-4650, Aug. 2012. doi:10.2514/6.2012-4650.

[3] Bach, R., "State Estimation Applications in Aircraft Flight-Data Analysis: A User's Manual for SMACK," NASA RP-1252, Mar. 1991.

[4] Morelli, E., and Klein, V., *Aircraft System Identification: Theory and Practice*, 2nd ed., Sunflyte Enterprises, Williamsburg, VA, 2016.

[5] Martos, B., and Morelli, E., "Using Indirect Turbulence Measurements for Real-Time Parameter Estimation in Turbulent Air," *Atmospheric Flight Mechanics Conference*, AIAA Paper 2012-4651, Aug. 2012. doi:10.2514/6.2012-4651.

[6] Martos, B., "Identifying and Correcting First Order Effects in Explanatory Variables for Longitudinal Real Time Parameter Identification Methods in Atmospheric Turbulence," Ph.D. thesis, University of Tennessee, Knoxville, Aug. 2013.

[7] Morelli, E., "System IDentification Programs for AirCraft (SIDPAC)," version 4.1, NASA Software Catalog, `http://software.nasa.gov`, accessed Oct. 2019.

[8] McRuer, D., Ashkenas, I., and Graham, D., *Aircraft Dynamics and Automatic Control*, Princeton University Press, Princeton, NJ, 1973, pp. 249–252.

[9] Etkin, B., "Turbulent Wind and Its Effect on Flight," *Journal of Aircraft*, Vol. 18, No. 5, 1981, pp. 327–345. doi:10.2514/3.57498.

[10] Nelson, R., *Flight Stability and Automatic Control*, McGraw-Hill, New York, NY, 1989, pp. 176–197.

[11] Klein, V., "Maximum Likelihood Method for Estimating Airplane Stability and Control Parameters From Flight Data in Frequency Domain," NASA TP-1637, May 1980.

[12] Clementson, G., "An Investigation of the Power Spectral Density of Atmospheric Turbulence," Ph.D. thesis, Massachusetts Institute of Technology, 1950.

[13] Chilton, R., "Some Measurements of Atmospheric Turbulence Obtained from Flow-Direction Vanes Mounted on an Airplane," NACA TN-3313, Nov. 1954.

[14] Notess, C., and Eakin, G., "Flight Test Investigation of Turbulence Spectra at Low Altitude Using a Direct Method for Measuring Gust Velocities," Cornell Aeronautical Laboratory Report No. VC-839-F-1, Jul. 1954.

[15] Grauer, J., "Position Corrections for Airspeed and Flow Angle Measurements on Fixed-Wing Aircraft," NASA TM-2017-219795, Nov. 2017.

[16] Morelli, E., "Real-Time Aerodynamic Parameter Estimation Without Air Flow Angle Measurements," *Journal of Aircraft*, Vol. 49, No. 4, 2012, pp. 1064–1074. doi:10.2514/1.C031568.

[17] Lanczos, C., *Applied Analysis*, Prentice Hall, Englewood Cliffs, NJ, 1956, pp. 331–336.

[18] Morelli, E., and Grauer, J., "Practical Aspects of Frequency-Domain Approaches for Aircraft System Identification," *Journal of Aircraft*, 2020. Accepted for publication.

[19] Anon., "Flying Qualities of Piloted Aircraft," US Department of Defense MIL-HDBK-1797, Dec. 1997.

[20] Bendat, J., and Piersol, A., *Random Data: Analysis and Measurement Procedures*, 2$^{\text{nd}}$ ed., John Wiley & Sons, Hoboken, NJ, 1986, pp. 130–132.

[21] Maine, R., and Iliff, K., "Maxmimum Likelihood Estimation of Translational Acceleration Derivatives from Flight Data," *Journal of Aircraft*, Vol. 16, No. 10, 1979, pp. 674–679. doi:10.2514/3.58588.

[22] Jategaonkar, R., and Gopalratnam, G., "Two Complementary Approaches to Estimate Downwash Lag Effects from Flight Data," *Journal of Aircraft*, Vol. 28, No. 8, 1991, pp. 540–542. doi:10.2514/3.46060.

[23] Grauer, J., Morelli, E., and Murri, D., "Flight-Test Techniques for Quantifying Pitch Rate and Angle-of-Attack Rate Dependencies," *Journal of Aircraft*, Vol. 54, No. 6, 2017, pp. 2367–2377. doi:10.2514/1.C034407.

[24] Etkin, B., *Dynamics of Flight*, John Wiley & Sons, New York, NY, 1959, pp. 153–165.